Theory of Strain-Controlled Magnetotransport and Stabilization of the Ferromagnetic Insulating Phase in Manganite Thin Films

Anamitra Mukherjee, William S. Cole, Patrick Woodward, Mohit Randeria, and Nandini Trivedi

Phys. Rev. Lett. **110**, 157201 — Published 9 April 2013

DOI: 10.1103/PhysRevLett.110.157201

Theory of strain controlled magnetotransport and stabilization of the ferromagnetic insulating phase in manganite thin films

Anamitra Mukherjee[1,2], William S. Cole[2], Nandini Trivedi[2], Mohit Randeria[2], and Patrick Woodward[3]
[1]*Department of Physics and Astronomy, University of British Columbia, Vancouver, BC V6T 1Z1, Canada,*
[2]*Department of Physics, The Ohio State University, Columbus, OH 43210, USA,*
[3]*Department of Chemistry, The Ohio State University, Columbus, OH 43210, USA*
(Dated: February 21, 2013)

We show that applying strain on half-doped manganites makes it possible to tune the system to the proximity of a metal-insulator transition, and thereby generate a colossal magnetoresistance (CMR) response. This phase competition not only allows control of CMR in ferromagnetic metallic manganites but can be used to generate CMR response in otherwise robust insulators at half doping. Further, from our realistic microscopic model of strain and magneto-transport calculations within the Kubo formalism, we demonstrate a striking result of strain engineering that under tensile strain a ferromagnetic charge ordered insulator, previously inaccessible to experiments, becomes stable.

Introduction.—Transition metal oxides have long been studied for their surprising emergent behavior such as high T_c superconductivity in the cuprates, ferroelectricity in the titanates, and colossal magnetoresistance (CMR) in the manganites. However, very recent advances in heterojunction growth [1–3] have opened the possibility of producing atomically perfect interfaces of oxide materials, and therefore applying precisely controlled strain to oxide thin films. In this Letter we address the impacts of strain on ordered phases, temperature scales, and CMR in the manganites. As a specific example, we consider materials at "half-doping" which have a prototypical chemical formula of $A_{0.5}A'_{0.5}MnO_3$ where A is a rare earth and A' an alkaline earth metal [4].

At large bandwidths (BW), the half-doped manganites are ferromagnetic metals (F-M), while narrow BW materials are spin, charge, and orbitally ordered insulators (SCO-I) as described later in the text. CMR is known to occur in F-M materials close to the metal-insulator phase boundary, and is the result of *phase competition* (between the F-M and a charge-ordered insulator), which is traditionally controlled by isovalent chemical substitutions at the A-site [4]. The unstrained material has been theoretically studied extensively [5, 6]. Most prior work on the effects of strain (both theory [7–13] and experiment [14–22]) have focused on how it affects the magnetic and electronic phases, with little emphasis on magnetotransport. We extend the usual model for manganites, previously used to study magnetotransport without strain [5, 6, 23], to propose and solve, for the first time, a microscopic Hamiltonian that includes the effects of strain and obtain the following results:

(i) Tensile strain provides a route to stabilizing a ferromagnetic charge ordered insulator (FC-I). This phase has not been conclusively observed in any half doped manganite with tolerance factor variations, but should finally be observable with strain engineering.

(ii) We demonstrate that strain can induce phase transitions. As a consequence, we show that the CMR in F-M materials can be enhanced by tuning the proximity to the metal-insulator transition, and that insulating phases can be made metallic under strain and therefore also exhibit a CMR response. This greatly expands the family of materials with potential device applications.

(iii) We show that strain engineering also allows for control over T_c in F-M manganites, and can be used to control the CMR temperature in the CMR materials.

Model.—We begin with the "standard model" for the manganites. Because of the octahedral crystal field, the Mn e_g levels have a higher energy than the t_{2g} levels. Combined with a large Hund's coupling, which ensures that the electron spins align ferromagnetically, this localizes three Mn $3d$ electrons in the t_{2g} levels which form local $S = 3/2$ moments (called "core spins"). The remaining electrons, if any, are itinerant and occupy two bands that result from the hybridization of the Mn e_g levels. The model also includes an effective antiferromagnetic superexchange J between neighboring Mn core spins, and finally the e_g electrons couple to Jahn-Teller phonons with a coupling strength λ.

All energy scales are given in units of the unstrained bandwidth t. This Hamiltonian yields an accurate description of the physics of the manganites [24] and is discussed in detail in the Supplementary Information section I.

We extend this model to incorporate the effects of strain. Fig. 1(a) schematically illustrates substrate-induced, in-plane tensile strain. Tensile (compressive) strain is caused by growing the film on substrates with lattice parameters larger (smaller) than those of the unstrained film. We assume that strain is applied parallel to the (a-b) plane, which we take to be the plane of the $d_{x^2-y^2}$ orbital. We quantify strain by the parameter $e_\parallel = [(a_s - a)/a] = \delta a/a$, where a_s and a are the substrate and film lattice parameters. Here a is the distance between two nearest neighbor Mn atoms. We consider volume conserving strain and use the relation $e_\perp = -4\nu e_\parallel$ where ν is the Poisson ratio. We choose $\nu = 0.375$, consistent with previous estimates [25, 26]. In-plane compressive strain corresponds to $e_\parallel < 0$, while $e_\parallel > 0$ for

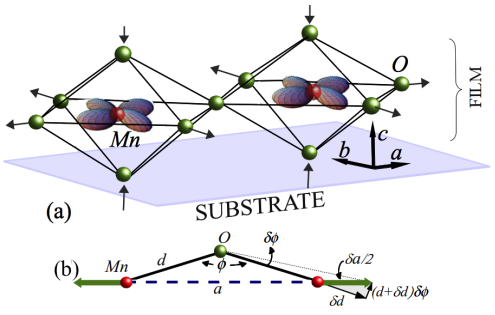

FIG. 1. (a) Uniform tensile strain in the a-b plane is introduced by lattice mismatch with the substrate. Volume conserving tensile strain expands the in-plane Mn-O bonds while contracting bonds in the c direction. This causes higher occupancy of the in-plane $d_{x^2-y^2}$ orbital, a larger out-of-plane hopping and smaller in-plane hopping compared to the unstrained values. Compressive strain, not shown, has the opposite effect. (b) Schematic of a generic Mn-O-Mn bond under strain. We indicate the Mn-O bond length d, Mn-O-Mn bond angle ϕ and the shortest Mn-Mn distance, the lattice parameter a. An expansion of a along the green arrows causes a change in d and ϕ.

tensile strain. With this in mind, we propose three microscopic effects of strain that must be included in our model, extending previous theoretical proposals [8, 9]:

(i) *Strain modifies the hopping matrix elements.* Strain affects the lattice parameter a which in turn modifies both the Mn-O bond length d and the Mn-O-Mn bond angle ϕ as seen in Fig. 1(b). In the Supplementary Information section I (c), we show by using Slater-Koster [27] and Harrison [28] scaling, that the effect on the hopping matrix elements due to the change in ϕ can be neglected for a large class of half doped manganites, and that the hopping in the (a-b) plane scales with strain as $t_{xy} \rightarrow t_{xy}\left(1-7e_{\parallel}\right)$. We restrict our calculations to a single layer manganite film in the a-b plane (as depicted in Fig. 1(a)) and refer to the unstrained in-plane hopping parameter t_{xy} as t, and under strain as $\tilde{t}$.

(ii) *Strain modifies the antiferromagnetic superexchange.* The superexchange coupling also scales with the hopping. From similar considerations it can be shown that the in-plane superexchange scales as $J_{xy} \rightarrow (J_{\parallel}/t)(1-14e_{\parallel})$ with strain. We refer to the unstrained in-plane superexchange as J and in the strained case, $\tilde{J}$.

(iii) *Strain generates an orbital bias.* Because of the increase in the in-plane Mn-O bond length, tensile strain makes occupation of the $d_{x^2-y^2}$ orbital energetically favorable. In-plane compressive strain favors the out-of-plane $d_{3z^2-r^2}$ orbital. This orbital bias induced by in-plane compressive and tensile strains in $La_{0.7}Sr_{0.3}MnO_3$ has been observed in x-ray absorption [29] as well as in angle resolved photoemission [30]. We incorporate this in our model Hamiltonian with an extra term, $H_{\rm bias} = \sum_{i,\alpha} \epsilon_\alpha n_{i,\alpha}$ where $\epsilon_\alpha = \delta/2$ for $\alpha = d_{3z^2-r^2}$ and $\epsilon_\alpha = -\delta/2$ for $\alpha = d_{x^2-y^2}$.

From experiments, the e_g splitting has been estimated to be between $0.4t$ and $3t$ [29, 31]. We make a conservative estimate for the bias to be $\delta \approx 10e_{\parallel}t$, i.e., a splitting of $\pm 0.2t$ for $\pm 2\%$ strain. These values are consistent with density functional estimates [32, 33]. Values of 2-3% for strain on manganite films, as we consider here, are easily achievable in experiments[15, 21].

As mentioned, we perform our calculations in two dimensions, describing a single-layer manganite film in the a-b plane. Further, we assume strain to be uniform in the layer. This is sufficient to bring out the important features of the phase diagram and in-plane transport. We describe our method of solution in Supplementary Information sections II and III and focus here on our results.

Strain driven phase transitions.—Fig. 2(b) shows the $T = 0$ $\lambda - J$ phase diagram without strain. On this we denote two representative parameter points, F-M (blue dot) and SCO-I (red dot). The SCO-I is an insulator with planar checkerboard charge order (CO), alternating $d_{x^2-r^2}/d_{y^2-r^2}$ orbital order (OO) (on the sites with larger charge density), and CE type spin order (zigzag ferromagnetic chains coupled antiferromagnetically). Fig. 2(a) and (c) show the effect of strain on these points.

Starting from these parameters, in-plane compressive strain favors F-M as seen in both (a) and (c). There are two competing effects here, however. Compressive strain increases the in-plane hopping which in turn reduces $\lambda/\tilde{t}$, as seen by following the dashed black arrow in (b). This favors a metallic state where double-exchange promotes ferromagnetism. On the other hand, compressive strain increases $\tilde{J}/\tilde{t}$, which tends to narrow the BW, while the orbital bias promotes occupancy of the out-of-plane $d_{3z^2-r^2}$ orbital. Both of these latter effects work against the stability of the F-M, but we find the F-M to be dominant up to the maximum values of strain we have considered.

In-plane tensile strain stabilizes insulators that can have either ferromagnetic or antiferromagnetic spin textures as seen in (a) and (c) respectively. The insulators have long-range checkerboard charge order and are stabilized by the reduced in-plane hybridization or increased $\lambda/\tilde{t}$, as seen by following the grey dashed arrow in (b). This effect tends to localize the electrons. While sufficient increase in λ eventually turns the system insulating regardless of the unstrained F-M parameter, the magnetic order depends crucially on the value of $\tilde{J}/\tilde{t}$.

This dependence of the magnetic/charge-ordering scales on strain has been seen in experiments, both away from [17] and at half-doping [15, 21]. They include increasing T_c with compressive strain in $a_{0.8}Ba_{0.2}MnO_3$, suppressing T_c with tensile strain in $La_{0.67}Ca_{0.33}MnO_3$, and increasing T_{CO} with tensile strain on $Pr_{0.5}Ca_{0.5}MnO_3$ [15, 21]. We note that while there is a dearth of experimental data on scaling of t and J for manganites, our results are robust to typical variations in the scaling [36].

Stability of the FC-I phase.—From Fig. 2 (b) we see

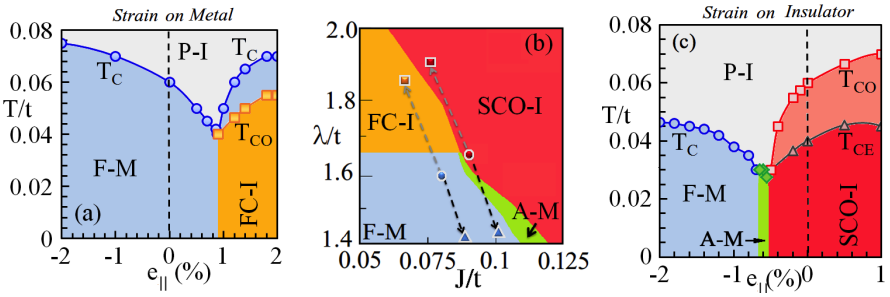

FIG. 2. (a) The ferromagnetic metal (F-M), ferromagnetic charge ordered insulator (FC-I), and paramagnetic insulator (P-I) in the temperature (T) vs. strain ($e_{\|}$) plane. Compressive strain ($e_{\|} < 0$) on F-M raises T_c, while tensile strain initially suppresses T_c but beyond $\sim 1\%$ strain drives the system into an FC-I. (b) Unstrained $T = 0$ phase diagram in the λ/t, J/t plane. This phase diagram also shows the spin-charge-orbital ordered insulator (SCO-I) and the A-type antiferromagnetic metal (A-M) [34]. The blue dot at (λ/t, J/t)=(1.6, 0.08) refers to the unstrained starting point from which we calculate (a), while the red dot at (λ/t, J/t)=(1.65, 0.09) refers to the unstrained point from which we calculate the phase diagram (c). Under strain, the hopping parameter t is rescaled which changes both the ratios λ/t and J/t. The symbols at the arrow heads indicate such values for 2% compressive (triangles) and tensile (squares) strain respectively. (c) Tensile strain on the SCO-I enhances charge ordering temperature T_{CO} while compressive strain causes a transition to F-M. T_{CE} denotes the spin ordering temperature. In (a) and (c), for clarity, we do not show strain-induced low temperature equilibrium phase separation [35].

that adequate tensile strain on F-M with J/t$\sim$0.05-0.08 convert the system into a FC-I, just as that depicted for ($\lambda/t = 1.6$, $J/t = 0.08$) by the grey dashed arrow. The unstrained FC-I phase, was predicted in theory [37] at λ, J values as in Fig. 2 (b). In small BW half-doped manganites, *e.g.* $La_{0.5}Ca_{0.5}MnO_3$, signatures of this phase coexisting with AF-CO phase were reported [38] at 90K. This implies that in the half-doped manganites either FC-I is the true ground state only in a narrow λ, J widow or it is a metastable state with energy very close to the true ground state. We predict that tensile strain on an ordered F-M suppresses other phases and can stabilize the FC-I as the ground state.

Effect of strain on magnetotransport.—The maximum CMR temperature achievable by BW tuned phase competition is the T_C of the unstrained material. Additionally, bicritical nature of the phase diagram and proximity to the metal-insulator boundary needed for CMR, keeps the T_C quite low [39]. We show that because strain affects different intrinsic energy scales differently, it not only tunes phase competition, but also allows optimization of the competition between CMR temperature and %MR.

Fig. 3(a) shows the resistivity, $\rho(T)$, for various tensile strain values on the unstrained F-M phase (blue dot in Fig. 2(b)). While CMR behavior has been reported before [5, 6, 9], our novelty is the use of strain as an external knob. Increasing tensile strain causes rapid rise in the resistivity maximum that occurs at $T \sim T_C$, accompanied with reduction of both the T_C and the temperature at the resistivity maximum (T_{CMR}). The reduction in T_C is due to the approach to the F-M/SCO-I boundary by increasing the tensile strain, as depicted in the inset in (a). The reason for the increase in the resistivity maximum is the strain-induced enhancement of metal-insulator coexistence at T_C as illustrated in (b).

The color maps here depict the volume fraction of the insulating regions (red patches) embedded in an otherwise conducting background at T_C. These insulating regions grow in volume with increasing strain and have short range (π, π) CO correlations; the same correlations that one finds in the competing FC-I phase. The thermal fluctuations at T_C are typically dominated by the nearest metastable minimum, in this case the FC-I phase. Further, since strain controls the proximity to the F-M/FC-I boundary, increasing tensile strain makes the FC-I state progressively approach the energy of the F-M ground state, favoring greater insulating regions with short range (π, π) CO correlations. If we start with other initial (unstrained) starting points, tensile strain can result in a F-M to SCO-I phase transition. The qualitative behavior of magnetotransport is the same as in the F-M to FC-I case shown here. Magnetotransport data near the FM/SCO-I phase boundary is shown in Supplementary Information Section IV.

In Fig. 3(c) we show the $\%MR$, defined as $100 \times [\rho(0) - \rho(h)]/\rho(0)$ and calculated at $T = T_{CMR}$, as a function of magnetic field for two cases. One shows %MR close to the F-M/FC-I phase boundary, with (circles) and without (diamonds) strain; the other shows %MR close to the F-M/SCO-I boundary. The amount of increase in the resistivity maximum with strain and the $\%MR$ depends on the domains of metastability of the competing phases, the type of the insulator and the largest tensile strain that can be applied before the system becomes insulating. However regardless of the nature of metal-insulator phase competition, applying tensile strain yields an enormous enhancement of %MR (circles and stars) over the unstrained values (diamonds and triangles).

Finally we demonstrate that *compressive* strain can drive insulators across the metal-insulator transition into the CMR regime. Fig. 4(a) shows $\rho(T)$ with increas-

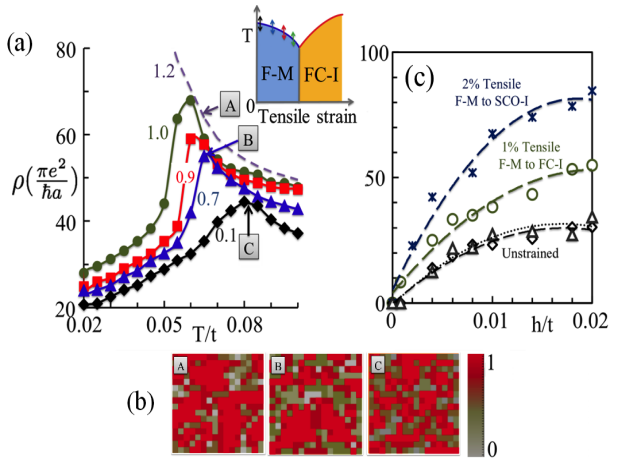

FIG. 3. (a) Resistivity $\rho(T)$ for different values of tensile strain. Strain values are marked on the individual curves, which are color coded with the arrows in the inset (which is a schematic of Fig. 2(a) showing only the tensile strain part). Note that while the temperature at which the peak occurs (which is close to T_C) decreases, the peak value of the resistivity increases. (b) Real space snapshots of charge ordering at T_C; the volume fraction of checkerboard charge ordered regions (shown in red) grows systematically with tensile strain. The labels A, B and C on them and in (a) denote the strain, temperature values where these were calculated. The magnetoresistance ($\%MR$) as a function of magnetic field for $\sim$1% strain on a system close to the F-M/FC-I phase boundary and $\sim$2% on a system close to the F-M/SCO-I boundary. The unstrained values for both parent parameter points (triangles and diamonds) are shown for comparison.

ing compressive strain on SCO-I. At 0.8% strain, the insulator-to-metal transition is accompanied by a CE-to-ferromagnetic transition. Increasing the compressive strain further causes a monotonic increase in T_C (also seen in the inset in (a)). The peak in the resistivity with increasing strain is also systematically shifted to higher temperatures. In (b) we plot %MR at the temperature of the resistivity maximum as a function of strain. We also show the corresponding CMR temperatures (T_{CMR}). We find that $\%MR$ is reduced upon increasing strain, as expected, but there is in fact an optimal region in which T_{CMR} can be increased without substantially reducing $\%MR$. We have checked that our results survive A site disordering.

Conclusion.—We stress a major difference between the strain engineering and isovalent substitution. While both can tune the bandwidth, uniform strain will not introduce the short-range disorder that naturally results from substitution. As a result, ferromagnetic T_C's and T_{CMR} of strained films should be higher than in their substitution-engineered counterparts. In turn, larger intrinsic bandwidth would cause greater %MR at smaller magnetic fields, since the external field required to align the core spins is reduced. Also, strain effects on manganites of any material composition and doping can be directly studied in our approach. Our results indicate some

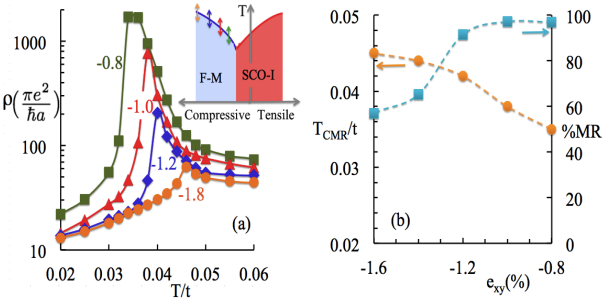

FIG. 4. Compressive strain can induce F-M in insulating manganites: (a) shows $\rho(T)$ of the resulting F-M as a function of temperature for various values of compression (color coded with the double arrows in the inset, which is a schematic of Fig. 2(c)). There is a pronounced peak which systematically shifts to higher temperatures with increasing compression. (b) Temperature at resistivity peak T_{CMR} (left axis), which increases with increasing compression, and %MR (right axis), which decreases as compression is increased. The %MR does not decrease drastically at first, and there is a region where T_{CMR} can be enhanced without losing the large %MR.

promising future directions. First, we have demonstrated that strain gives access to a large phase space of new and accessible states for a given unstrained material. Second, strain need not introduce disorder, in contrast to chemical substitution. Finally, strain directly impacts orbital occupancy in a tunable way, and opens new possibilities for orbital-state sensitive electronics.

We gratefully acknowledge support from DOE DE-FG02-07ER46423 (A.M.), DOE BES DE-SC0005035 (M.R.), NSF DMR-0907275 (N.T.), and Center for Emergent Materials, NSF MRSEC DMR-0820414 (W.S.C. and P.W.).

[1] J. Mannhart *et al.*, Science **327**, 1607 (2010).
[2] E. Dagotto, Science **318**, 1076 (2007).
[3] H. Y. Hwang *et al.*, Nature Materials **11**, 103 (2012).
[4] D. Akahoshi *et al.*, Phys. Rev. Lett. **90**, 177203 (2003).
[5] C. Şen *et al.*, Phys. Rev. Lett. **105**, 097203 (2010).
[6] C. Şen *et al.*, Phys. Rev. Lett. **98**, 127202 (2007).
[7] K. H. Ahn *et al.*, Nature **428**, 401 (2004).
[8] A. Baena *et al.*, Phys. Rev. B **83**, 064424 (2011).
[9] S. Dong *et al.*, Phys. Rev. B **82**, 035118 (2010).
[10] J. H. Lee *et al.*, Phys. Rev. Lett. **104**, 207204 (2010).
[11] K. H. Ahn *et al.*, Physical Review B **64**, 115103 (2001).
[12] A. J. Millis *et al.*, Journal of Applied Physics **83**, 1588 (1998).
[13] M. J. Caldern *et al.*, Physical Review B **68**, 100401 (2003).
[14] F. Yang *et al.*, Appl. Phys. Lett. **97**, 092503 (2010).
[15] D. Okuyama *et al.*, Appl. Phys. Lett. **95**, 152502 (2009).
[16] J. Wang *et al.*, Appl. Phys. Lett. **96**, 052501 (2010).
[17] H. Chou *et al.*, Appl. Phys. Lett. **89**, 082511 (2006).
[18] C. K. Xie *et al.*, Appl. Phys. Lett. **93**, 182507 (2008).
[19] V. Pena *et al.*, Journal of Physics and Chemistry of Solids **67** (2006).
[20] S. de Brion *et al.*, Journal of Magnetism and Magnetic Materials **272** (2004).
[21] Z. Q. Yang *et al.*, Applied Physics Letters **88**, 072507 (2006).
[22] Y. Konishi *et al.*, J. Phys. Soc. Jpn. **68**, 3790 (1999).
[23] R. Yu *et al.*, Phys. Rev. B **77**, 214434 (2008).
[24] E. Dagotto *et al.*, Physics Reports **344**, 1 (2001).
[25] H. Yamada *et al.*, Appl. Phys. Lett. **89**, 052506 (2006).
[26] C. Adamo *et al.*, Appl. Phys. Lett. **95**, 112504 (2009).
[27] J. C. Slater and G. F. Koster, Phys. Rev. **94**, 1498 (1954).
[28] W. Harrison, *Electronic Structure and the Properties of Solids: The Physics of the Chemical Bond, Dover* (1989).
[29] C. Aruta *et al.*, Phys. Rev. B **73**, 235121 (2006).
[30] A. Tebano *et al.*, Phys. Rev. B **82**, 214407 (2010).
[31] A. Tebano *et al.*, Phys. Rev. B **74**, 245116 (2006).
[32] B. R. K. Nanda *et al.*, Phys. Rev. B **78**, 054427 (2008).
[33] B. R. K. Nanda *et al.*, Phys. Rev. B **81**, 174423 (2010).
[34] K. Pradhan *et al.*, Phys. Rev. Lett. **99**, 147206 (2007).
[35] At low temperatures ($T \sim 0.005t$) strain causes phase separation between F-M and SCO-I or FC-I, as seen in experiments [19, 20, 31] and theory [7]. However, with increasing temperature, such phase separated states rapidly evolve either into a global F-M or SCO-I phase and do not affect our finite temperature results..
[36] Using t$\sim d^{-2}$ and J$\sim d^{-4}$ known for La_2CuO_4 [40], only causes quantitative changes. It shifts the metal-insulator transition in Fig 2 (a) to 2% tensile strain and that in Fig 2 (b) to about 2.5% compressive strain. These changes are small enough so that our results are still easily accesible to experiments.
[37] S. Yunoki *et al.*, Physical Review Letters **84**, 3714 (2000).
[38] J. C. Loudon *et al.*, Nature **420**, 797 (2002).
[39] Y. Tokura, *Colossal Magnetoresistive Oxides, Gordon and Breach, Amsterdam* (2000).
[40] S. L. Cooper, G. A. Thomas, A. J. Millis, P. E. Sulewski, J. Orenstein, D. H. Rapkine, S.-W. Cheong, and P. L. Trevor, Phys. Rev. B **42**, 10785 (1990).